

Vaughn, L.W., Leary, R.J., and Read, M.T., 2022, Tectonic and stratigraphic evolution of the late Paleozoic Darwin Basin, eastern California, USA, and implications for the onset of subduction along the southwestern Cordilleran margin of Laurentia: GSA Bulletin, <https://doi.org/10.1130/B36664.1>.

Supplemental Material

Text. Field Methods, Detailed Methods for Conodont Biostratigraphy, Clast Counting Methods, and Detailed Methods for Tectonic Subsidence Analysis.

Figure S1. Measured sections 1.2 and 1.3 at the mouth of Osborne Canyon (Lower Osborne Canyon). Section 1.2 traverses the uppermost part of the Tihvipah Limestone (IPt) and the Osborne Canyon Formation (Po). Section 1.3 traverses an incomplete faulted section of the Osborne Canyon Formation. Both sections terminate at faults. See Figure 4.1 for traverse locations and Fig. 5 for legend.

Figure S2. Measured sections 2.1 and 2.2 in the southernmost Darwin Hills. Section 2.1 traverses the Mississippian Indian Springs Formation (Mi), Pennsylvanian Tihvipah Limestone (IPt), and unit 1 of the Darwin Hills sequence (IPdh1). The former two are separated from the latter by an angular unconformity. Section 2.2 traverses the Mississippian Indian Springs Formation (Mi), Pennsylvanian Tihvipah Limestone (IPt), and units 3-6 of the Darwin Hills sequence (IPdh3-PIPdh6). Both sections terminate at Quaternary Alluvium. See Figure 4.5 for traverses and Fig. 5 for legend. See Table S2 for clast count data.

Figure S3. Measured sections 5.1, 5.2, 5.3, and 5.4 in the Santa Rosa Hills. Sections traverse the uppermost part of the Tihvipah Limestone (IPt), and the exposed portion of the unnamed turbidite unit (PIPut). Sections end where Quaternary alluvium obscures further section. See Figure 4.5 for traverses and Fig. 5 for legend. See Table S2 for clast count data.

Figure S4. 30 hypothetical subsidence curves for the Darwin Basin. The curves plotted in black and white are presented in the main paper. Plotted in blue, green, and red are the calculated subsidence curves assuming low, moderate, and high, respectively, paleobathymetry estimates. Shaded in gray is the possible range of subsidence curves for the Darwin Basin. Regardless of the absolute magnitude of paleobathymetry (except for perhaps the high-end estimates), or how paleobathymetric increase varies over time (i.e., linear, logarithmic, exponential), all 30 curves have similar concave down geometry and display initially gradual subsidence before an abrupt transition to rapid subsidence. Based on this, we are confident about drawing conclusions about the evolution of the Darwin Basin based on the geometry of these curves. See Table S3 for values used in constructing these curves.

Table S1. Sample list.

Table S2. Clast counts.

Table S3. Parameters used in subsidence analysis including paleobathymetry estimates.

1 Tectonic and stratigraphic evolution of the late Paleozoic
2 Darwin Basin, eastern California, USA, and implications
3 for the onset of subduction along the southwestern
4 Cordilleran margin of Laurentia – Supplemental Data File

5
6 **L. W. Vaughn¹, Ryan J. Leary¹, Michael T. Read²**

7 *¹Department of Earth and Environmental Science, New Mexico Institute of Mining and
8 Technology, 801 Leroy Pl, Socorro, NM 87801, USA*

9 *²Department of Geology, Stephen F. Austin State University, 2102 Alumni Dr,
10 Nacogdoches, TX 75962, USA*

11 **FIELD METHODS**

12 During this study, we measured 15 sections, but only presented the most important
13 sections in the main manuscript. The remainder are included in this supplemental data
14 file (**Fig. S1, S2, and S3**).

15 **DETAILED METHODS FOR CONODONT BIOSTRATIGRAPHY**

16 Conodont elements were picked following chemical digestion of carbonate samples and
17 density separation of the resultant insoluble residues. Prior to chemical processing, bulk
18 samples were broken into small pieces (between two and six centimeters in diameter),
19 rinsed thoroughly to remove any coating of carbonate dust, and digested using a
20 buffered 8-10% formic acid solution. The formic acid solution was changed every 1.5

21 days and the digestion process was repeated until nearly all acid-soluble material was
22 dissolved. The remaining insoluble residues were sieved between 16 and 120 meshes
23 and collected with each changing of the buffered acid solution. Care must be taken
24 when sieving insoluble residues to avoid damaging any conodont elements present.
25 Complete digestion of a three to five-kilogram carbonate or mixed carbonate-siliciclastic
26 sample typically requires seven to ten days of continuous chemical processing.

27

28 Insoluble residues were dried in an oven at low temperature (50° C) to avoid thermal
29 alteration of low-CAI (conodont color alteration index) specimens. The heavy mineral
30 fraction of the insoluble residue was then density separated from quartz grains and
31 other “light” insolubles using separation funnels and a solution of tetrabromoethane and
32 acetone measured to a density of 2.81 to 2.83 g/ml. Separation funnels were covered
33 and stirred twice daily for two to three days. Once captured, the heavy fraction was
34 rinsed with acetone and left to dry for several days. Samples remained under a fume
35 hood until they were completely odorless. See **Table S1** for sample locations and
36 information.

37 **CLAST COUNTING METHODS**

38 We counted between 84 to 210 clasts in 15 beds of calcirudite in the Darwin Basin. The
39 number of clasts counted varied based on the grain size and exposure of the bed.
40 Counting was done by choosing an initial starting clast, and then counting adjacent
41 clasts in an outward spiral from the first clast. See **Table S2** for clast count data.

42 **DETAILED METHODS FOR TECTONIC SUBSIDENCE ANALYSIS**

43 One-dimensional subsidence analysis is a quantitative technique that reconstructs the
 44 vertical displacement of a point on an initially horizontal datum through time, based on
 45 information extracted from the stratigraphic column overlying this horizontal datum
 46 (Steckler and Watts, 1978; van Hinte, 1978; Sclater and Christie, 1980; Bond and
 47 Kominz, 1984; Dickinson et al., 1987; Angevine et al., 1990; Roberts et al., 1998; Xie
 48 and Heller, 2009; Allen and Allen, 2013; Sturmer et al., 2018; Lee et al., 2018).
 49 Computing the vertical displacement (i.e., subsidence and/or uplift) of such a point at
 50 any time in the past, t , is a multi-step process that requires information about the
 51 thickness, lithology, and age of the stratigraphy overlying the datum, the paleo-
 52 bathymetry or paleo-elevation at which deposition of these sediments occurred, and
 53 eustatic variation in sea level between t and the present day. The process of calculating
 54 vertical displacement at any time, t , begins by restoring the thickness of the stratigraphic
 55 column overlying the point to its thickness at t by undoing post- t diagenetic processes
 56 that resulted in thickness changes such as compaction or pressure solution (e.g. Sclater
 57 and Christie, 1980). The decompaction equation (Allen and Allen, 2013) must be solved
 58 iteratively for each unit in the overlying stratigraphy:

$$59 \quad y'_2 - y'_1 = y_2 - y_1 - \frac{\phi_0}{c} [e^{-cy_1} - e^{-cy_2}] + \frac{\phi_0}{c} [e^{-cy'_1} - e^{-cy'_2}] \quad (\text{S1})$$

60 Where y_2 and y_1 are the present day burial depths of the base and top of the unit being
 61 decompacted, ϕ_0 is the initial porosity of the sediment that makes up the unit at the
 62 moment of deposition, typically obtained by comparison with modern sediments (**Table**
 63 **2**), c is an empirically derived porosity decay constant (**Table 2**) and y'_2 and y'_1 are the
 64 burial depths of the base and top of the unit in question after removing overlying strata

65 and decompacting the unit by this process. Next the porosity Φ of each restored
66 sedimentary layer must be calculated following Athy, (1930) and Allen and Allen,
67 (2013):

$$68 \quad \Phi = \frac{\Phi_0}{c} * \frac{e^{-cy'_1} - e^{-cy'_2}}{y'_2 - y'_1} \quad (S2)$$

69 A component of subsidence undergone by the point in question will be caused by
70 localized flexural loading due to the weight of the stratigraphic column on the
71 lithosphere at the point; but this component can be calculated and removed via a simple
72 isostatic balancing process called backstripping (e.g. Steckler and Watts, 1978; Allen
73 and Allen, 2013), which first requires the calculation of the density of the sedimentary
74 column using the restored thickness calculated in **Equation S1** and the porosity
75 calculated by **Equation S2**:

$$76 \quad \bar{\rho}_s = \sum_i \left\{ \frac{\bar{\phi}_i(\rho_w) + (1 - \bar{\phi}_i)\rho_{sg_i}}{S} \right\} y'_i \quad (S3)$$

77 From Steckler and Watts, (1978) where $\bar{\phi}_i$ is the porosity of the *i*th layer, ρ_w is the
78 density of water (1025 kg/m³ for sea water, Lee et al., 2019), ρ_{sg_i} is the density of the
79 individual framework grains that make up the *i*th sedimentary layer (**Table 2**), y'_i is the
80 restored thickness of the *i*th sedimentary layer, and S is the restored thickness of the
81 entire sedimentary column. Once the density of the sedimentary column is known, the
82 backstripped tectonic subsidence (i.e. subsidence caused solely by tectonic processes
83 such as flexural loading of the lithosphere in an orogenic belt or isostatic adjustment

84 following thinning of the lithosphere in a rift, e.g. Steckler and Watts, 1978; Xie and
85 Heller, 2009; Allen and Allen, 2013) is given by:

$$86 \quad Z(t) = S(t) \left(\frac{\rho_m - \rho_s}{\rho_m - \rho_w} \right) + W_d(t) \pm \Delta_{SL}(t) \left(\frac{\rho_m}{\rho_m - \rho_w} \right) \quad (S4)$$

87 From Steckler and Watts, (1978), where $Z(t)$ is the tectonic subsidence at any time t ,
88 $S(t)$ is the decompacted sediment layer thickness at t , ρ_m is the density of the mantle
89 (3300 kg/m^3 , Lee et al., 2019), $W_d(t)$ is the paleo-bathymetry or paleo-elevation of
90 deposition at t (**Table 2**), and Δ_{SL} is the difference between eustatic sea level at t and
91 mean sea level at the present time. Computation of $Z(t)$ at a series of times yields a
92 tectonic subsidence curve which illustrates the component of subsidence of the point
93 caused purely by tectonic forces. The geometry, slope, duration, and concavity (and
94 abrupt changes in these features) of the resulting curve can be used to speculate on the
95 timing and mechanism by which tectonic subsidence occurred (Bond and Kominz, 1984;
96 Bond et al., 1985; Xie and Heller, 2009; Allen and Allen, 2013; Lee et al., 2018).

97 At the time of this study, we have sufficient data to produce one-dimensional, Airy-type
98 tectonic subsidence curves (e.g., Steckler and Watts, 1978; van Hinte, 1978; Sclater
99 and Christie, 1980; Bond and Kominz, 1984; Dickinson et al., 1987; Hegarty et al.,
100 1988; Angevine et al., 1990; Roberts et al., 1998; Xie and Heller, 2009; Allen and Allen,
101 2013; Sturmer et al., 2018) for three locations within the Darwin Basin. The duration of
102 our curves includes both the Darwin Basin and pre-Darwin Basin Pennsylvanian shelf.
103 Polyphase deformation of Darwin Basin strata and limited along-strike and along-dip
104 exposure of the basin preclude the construction of more advanced subsidence models

105 (e.g., Roberts et al., 1998). Iterative decompaction and backstripping (e.g., Steckler and
106 Watts, 1978; Sclater and Christie, 1980) calculations were completed using the program
107 Backstrip (Nestor Cardozo, <http://www.ux.uis.no/~nestor/work/programs.html>).

108 Stratigraphic thicknesses were compiled from Stone et al. (1987; 2014); Stevens et al.
109 (2015c) and this study (**Table 2**). Age control was introduced by comparing
110 biostratigraphic data in Stone et al. (2014); Stevens et al. (2015a; 2015c), and our new
111 data from this study with the timescales of Aretz et al., (2020) and Henderson et al.,
112 (2020) (**Fig. 3 and Table 2**). Informed by our petrographic examination of Darwin Basin
113 strata, we picked reasonable grain density values, exponential porosity decay
114 constants, and initial porosity values for rocks of the Darwin Basin from those reported
115 for similar lithofacies described by Sclater and Christie (1980, and references therein)
116 and Hegarty et al. (1988) (**Table 2**). When choosing values for these terms we assumed
117 that all porosity loss in the Darwin Basin occurred via compaction and/or pressure
118 solution, that abnormally early cementation did not occur (e.g., Bond and Kominz,
119 1984), and that Darwin Basin strata were normally pressured during burial. Pressure
120 solution features at both the outcrop and thin section scale are ubiquitous within the
121 Darwin Basin. Following the approach of Xie and Heller, (2009) we chose to ignore
122 eustatic sea level variation in construction of our curves because these variations are
123 poorly constrained, especially during the late Paleozoic (e.g., Ross and Ross, 1987;
124 Dyer and Maloof, 2015), but more importantly because the plausible range in magnitude
125 of this variation in sea level, perhaps 200 meters across the entire late Paleozoic, is an
126 order of magnitude smaller than the thickness of sediment deposited within the Darwin
127 Basin (**Table 2**). In other words, over ten Myr a few tens of meters of eustatic sea level

128 variation is insignificant in comparison to the deposition of few thousand meters of
129 sediment and hundreds of meters of paleobathymetric variation.

130 The foremost obstacle to one-dimensional tectonic subsidence analysis lies in the
131 accurate estimation of the paleo-bathymetry or paleo-elevation at which deposition
132 occurred (e.g., Dickinson et al., 1987; Roberts et al., 1998; Xie and Heller, 2009). Errors
133 resulting from inaccurate paleo-bathymetry or elevation estimates are small in shallow
134 marine or terrestrial basins but can be significant in deep-marine settings such as the
135 Darwin Basin (Dickinson et al., 1987; Xie and Heller, 2009). Reasonable paleo-
136 bathymetry estimates of deep-water strata based on facies analysis (e.g., Angevine et
137 al., 1990) can vary by over an order of magnitude. For example, in the modern oceans,
138 essentially identical deep water carbonate depositional systems can exist anywhere
139 from a few hundred meters to several kilometers water depth (Payros and Pujalte, 2008;
140 Reijmer et al., 2015; Mulder et al., 2017; Tournadour et al., 2017). This problem is
141 compounded by the fact that no *in situ* fossils that could be used to estimate paleo-
142 bathymetry are present in Darwin Basin strata. For these reasons we have devised two
143 methods for constraining paleobathymetry in our model. For one approach we have
144 assumed no change in paleobathymetry during deposition of Darwin Basin and older
145 Pennsylvanian shelf strata. Although this assumption is almost certainly violated based
146 on lithofacies analysis of Darwin Basin strata, we argue that this is the most
147 conservative and justifiable approach to constraining paleo-bathymetry in the Darwin
148 Basin. This approach precludes overestimation of tectonic subsidence, prevents the
149 presentation of artificial subsidence or uplift caused by inaccurate paleo-bathymetry
150 picks, and provides a firm, minimum bound on variation in our subsidence curves. In

151 other words, the true magnitude and rate of subsidence within the Darwin Basin must
152 necessarily be equal to, or greater than, the subsidence illustrated by our model. We
153 have thus used this approach for the subsidence curves presented in the main body of
154 this paper.

155 The second approach strengthens the conclusions we draw in the main paper regarding
156 the geometry of our subsidence curves. We argue that a simple mathematical
157 assumption based on lithofacies analysis limits variation in the geometry of our curves
158 to vertical uncertainty alone. We illustrate this below to support our conclusions in the
159 main paper. Let W_{db} equal the paleobathymetry, in meters, at which the Bird Spring
160 Formation was deposited, W_{dt} equal the paleobathymetry at which the Tihvipah
161 Limestone was deposited, W_{do} equal the paleobathymetry at which the Osborne
162 Canyon Formation was deposited, and W_{dd} equal the paleobathymetry at which the
163 Darwin Canyon Formation was deposited. Based on lithofacies analysis, it is clear that
164 the deep-marine facies of the Darwin Canyon and Osborne Canyon formations were
165 deposited in deeper water than slope facies of the Tihvipah Limestone, that in turn were
166 deposited in deeper water than shelf facies of the Bird Spring Formation. Despite our
167 inability to quantify the exact paleo-bathymetry at which deposition occurred, we can
168 express this mathematically as:

$$169 \quad W_{db} < W_{dt} < W_{do} < W_{dd} \quad (1)$$

170 Xie and Heller (2009) proposed an average paleo-bathymetry of 150 meters for shelf
171 environments and 350 meters for upper slope depositional environments; in absence of
172 other constraints for the paleobathymetry of these units, we can assume a similar paleo-

173 bathymetry of deposition for the shelf and slope facies of the Bird Spring Formation and
174 Tihvipah Limestone. Next, based on the large amount of calciclastic detritus in all units
175 of the Darwin Basin, we can place a lower bound on **Equation 1** by assuming that
176 deposition of the Darwin Canyon and Osborne Canyon formations occurred above the
177 carbonate compensation depth. The depth of the carbonate compensation depth in the
178 late Paleozoic is unknown, but over Cenozoic times the carbonate compensation depth
179 has varied between 3 and 4.6 kilometers in the equatorial Pacific Ocean (Pälike et al.,
180 2012). Because the Darwin Basin formed at equatorial latitudes on the eastern margin
181 of the Panthalssan Ocean, we can adopt a conservative estimate of 3 kilometers for the
182 CCD. The adoption of the CCD as the lower bound on our equation is somewhat
183 arbitrary, as nearly any reasonable paleobathymetry value produces similar results
184 when applied as the lower bound (**Fig. S4**) Applying these bounds to **Equation 1** results
185 in:

$$186 \quad 150 < 350 < W_{do} < W_{dd} < 3000 \quad (2)$$

187 We envisioned three possible scenarios to describe how paleobathymetry in the Darwin
188 Basin increased over time between the lower and upper bounds of **Equation 2**. 1.
189 Paleobathymetry increased at a constant rate. 2. The rate at which paleobathymetry
190 increased, increased with time. 3. The rate at which paleobathymetry increased,
191 decreased with time. We applied linear interpolation (scenario 1), exponential
192 regression (scenario 2), and logarithmic regression (scenario 3) to **Equation 2** and thus
193 calculated hypothetical paleobathymetry of deposition values (see **Table S3**) for deep-
194 marine strata of the Darwin Basin (W_{do} , W_{dd}). For each method, we further envisioned a

195 high-end (3 km, conservative estimate of CCD), moderate (2 km, arbitrary, for
196 illustrative purposes only), and low-end estimate (1 km, arbitrary, for illustrative
197 purposes only) of paleobathymetry of deposition for the Darwin Canyon Formation.
198 These estimates, including the CCD, are somewhat arbitrary but fall within realistic
199 bathymetry ranges for modern deep-marine carbonate depositional systems. However,
200 these paleobathymetric estimates are not intended to be and should not be considered
201 as the actual depth at which the Darwin Canyon Formation was deposited. They are
202 convenient lower bounds to our interpolation/regression and serve only to illustrate our
203 assumptions, and support the conclusions presented in the main paper.

204 Producing subsidence curves using the moderate and low-end estimated
205 paleobathymetry values results in subsidence curves (Blue and Green in **Fig. S4**) with
206 similar geometry and concavity compared to the curves we present in this paper, but
207 progressively steeper slopes as increasing values of paleobathymetry are used. The
208 high-end estimate paleobathymetry curves (red in **Fig. S4**) are less similar, as the
209 geometry and concavity of these curves are drowned out by exceptionally high
210 subsidence rates. However, based on the constant overall geometry (concave down,
211 initially gradual subsidence followed by an abrupt transition to rapid subsidence) of all
212 the other curves, we are confident in drawing conclusions about the tectonic origin and
213 history of the Darwin Basin based on the geometry of these curves (detailed in main
214 paper). Finally, we argue that the true subsidence curve of the Darwin Basin must lie
215 between the deepest high-end estimate and the shallowest low-end estimate
216 (somewhere in the gray shaded field in **Fig. S4**), and its overall geometry must mimic

217 the other illustrated curves, (i.e. concave down, initial gradual subsidence, and later
218 rapid subsidence).

219 SUPPLEMENTAL FIGURE CAPTIONS

220 **Figure S1:** Measured sections 1.2 and 1.3 at the mouth of Osborne Canyon (Lower
221 Osborne Canyon). Sections 1.2 traverses the uppermost part of the Tihvipah Limestone
222 (IPt) and the Osborne Canyon Formation (Po). Section 1.3 traverses an incomplete
223 faulted section of the Osborne Canyon Formation. Both sections terminate at faults. See
224 **Figure 4.1** for traverse locations and **Fig. 5** for legend. C—clay; vF—very fine sand;
225 M—medium sand; vC—very coarse sand; P—pebble; B—Boulder.

226 **Figure S2:** Measured sections 2.1 and 2.2 in the southernmost Darwin Hills. Section
227 2.1 traverses the Mississippian Indian Springs Formation (Mi), Pennsylvanian Tihvipah
228 Limestone (IPt), and unit 1 of the Darwin Hills sequence (IPdh1). The former two are
229 separated from the latter by an angular unconformity. Section 2.2 traverses the
230 Mississippian Indian Springs Formation (Mi), Pennsylvanian Tihvipah Limestone (IPt),
231 and units 3-6 of the Darwin Hills sequence (IPdh3-PIPdh6). Both sections terminate at
232 Quaternary Alluvium. See **Figure 4.5** for traverses and **Fig. 5** for legend. See **Table S2**
233 for clast count data. C—clay; vF—very fine sand; M—medium sand; vC—very coarse
234 sand; P—pebble; B—Boulder.

235 **Figure S3:** Measured sections 5.1, 5.2, 5.3, and 5.4 in the Santa Rosa Hills. Sections
236 traverse the uppermost part of the Tihvipah Limestone (IPt), and the exposed portion of
237 the unnamed turbidite unit (PIPut). Sections end where Quaternary alluvium obscures

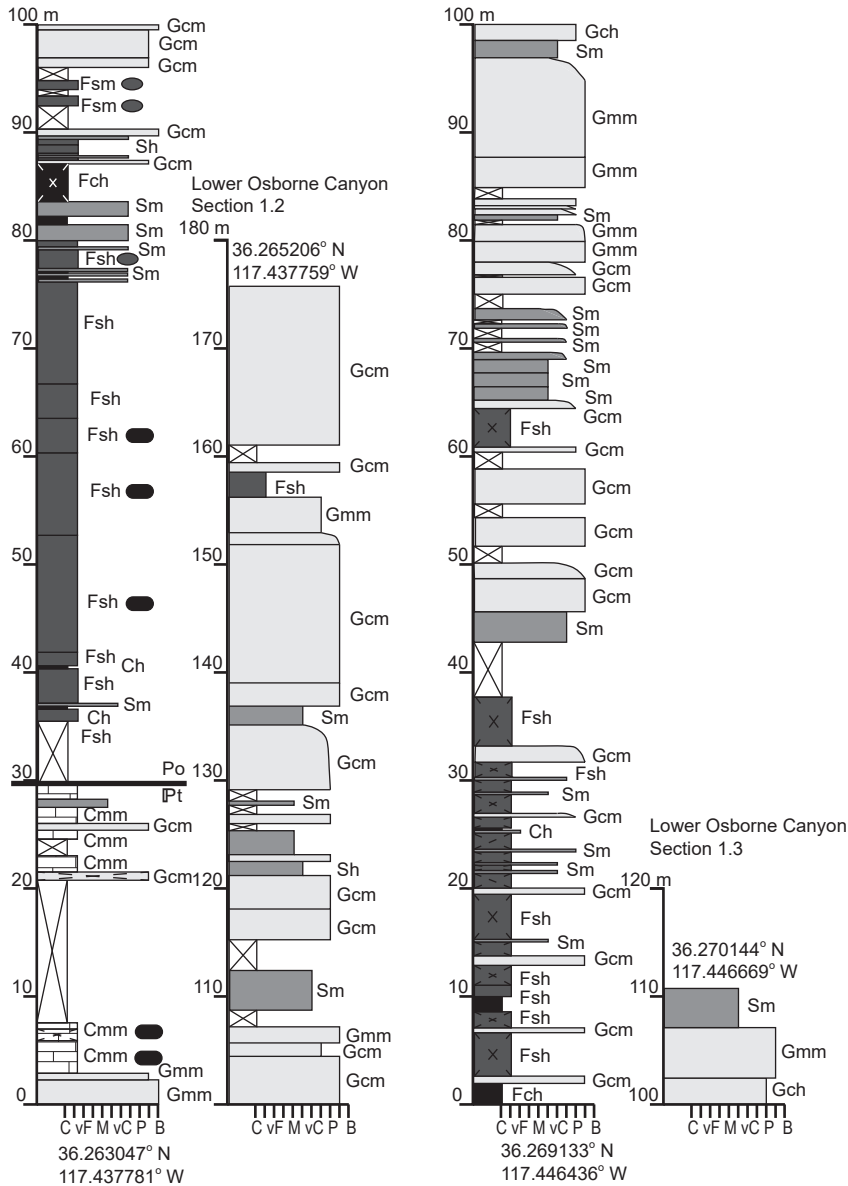
238 further section. See **Figure 4.5** for traverses and **Fig. 5** for legend. See **Table S2** for
239 clast count data. C—clay; vF—very fine sand; M—medium sand; vC—very coarse
240 sand; P—pebble; B—Boulder.

241
242 **Figure S4:** 30 hypothetical subsidence curves for the Darwin Basin. The curves plotted
243 in black and white are presented in the main paper. Plotted in blue, green, and red are
244 the calculated subsidence curves assuming low, moderate, and high, respectively,
245 paleobathymetry estimates. Shaded in gray is the possible range of subsidence curves
246 for the Darwin Basin. Regardless of the absolute magnitude of paleobathymetry (except
247 for perhaps the high-end estimates), or how paleobathymetric increase varies over time
248 (i.e., linear, logarithmic, exponential), all 30 curves have similar concave down geometry
249 and display initially gradual subsidence before an abrupt transition to rapid subsidence.
250 Based on this, we are confident about drawing conclusions about the evolution of the
251 Darwin Basin based on the geometry of these curves. See **Table S3** for values used in
252 constructing these curves.

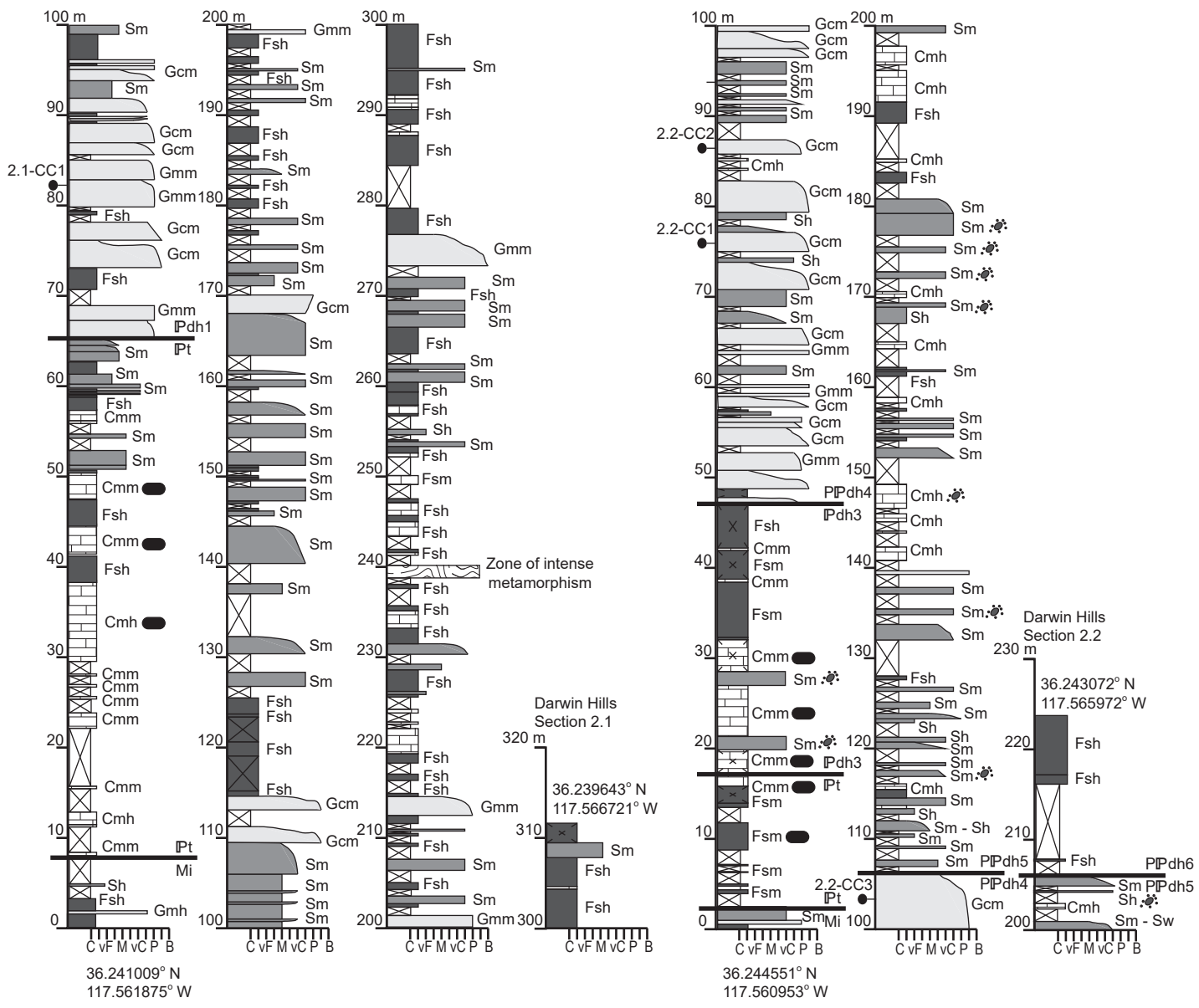
253 **SUPPLEMENTAL REFERENCES**

254 Athy, L.F., 1930, Density, Porosity, and Compaction of Sedimentary Rocks: AAPG
255 Bulletin, v. 14, p. 1-24.

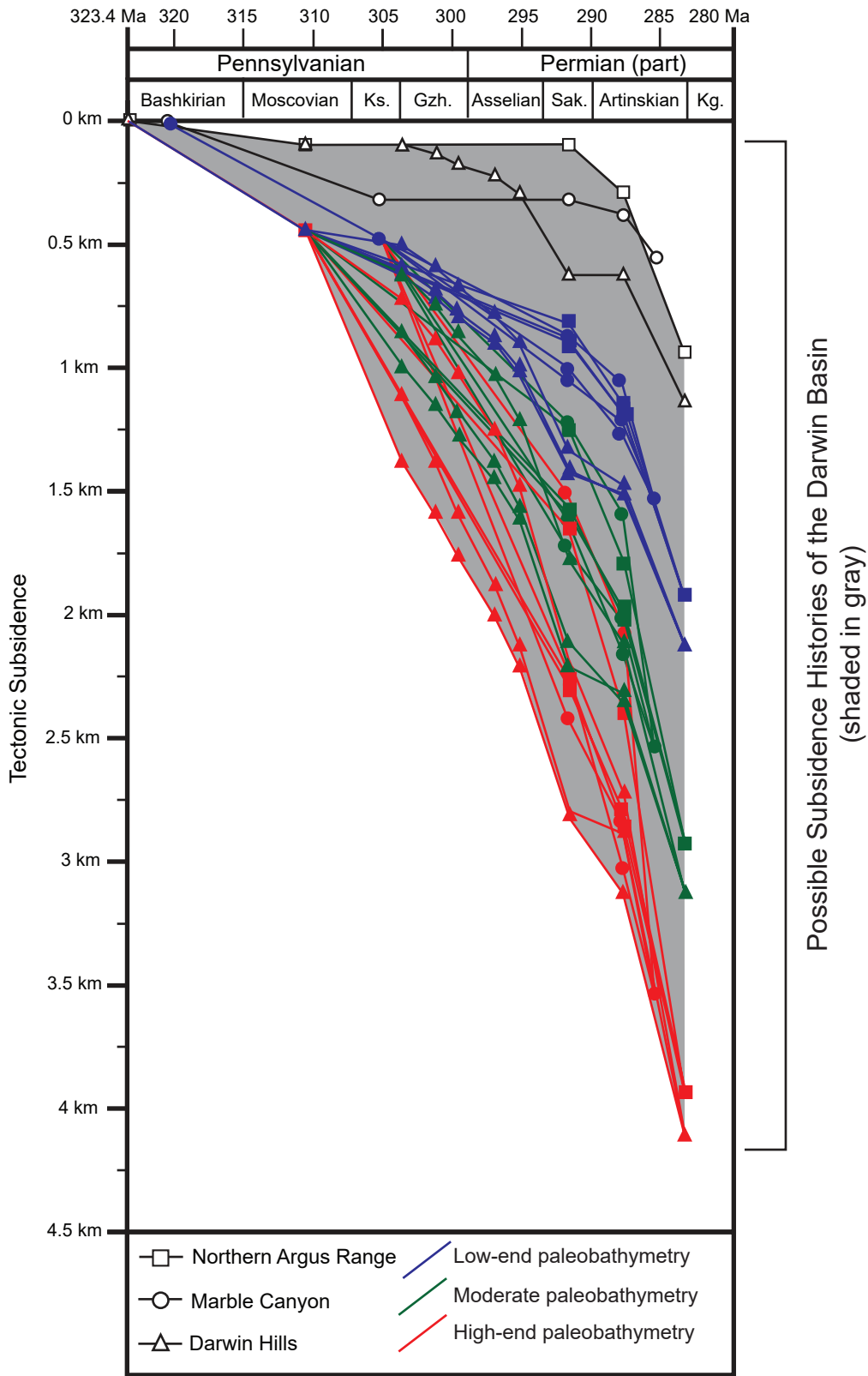
256 Pälke, H., and 64 others, 2012, A Cenozoic record of the equatorial Pacific carbonate
257 compensation depth: Nature, v. 488, p. 609–614, doi:10.1038/nature11360.



Vaughn et al. Figure S1



Vaughn et al. Figure S2



Vaughn et al. Figure S4